JOURNAL OF MATERIALS SCIENCE 30 (1995) 1259–1265

Effect of pH and hydrogen peroxide in radioactive water on the passivity of 1018 carbon steel

G. BELLANGER*
Commissariat à l'Energie Atomique, Centre d'Etudes de Valduc, F21120 Is sur Tille, France

Tritiated water, containing radiolytic hydrogen peroxide, was used in this work. In the vessels of the plant for the reprocessing of this water, the pH necessarily has different values, and consequently, we used pH values of 5–6 and 13 in our studies. The corrosion potential of the carbon steel, as well as the redox potential of the tritiated water taken immediately from a closed storage vessel with a pressure of 5×10^5 Pa radiolytic gas, are in the passive–transpassive potentials. Immediately after removal from storage, the concentration of hydrogen peroxide decreases rapidly and the potentials are in the prepassive region. This will subsequently reveal the importance of the concentration of radiolytic hydrogen peroxide in passivity and corrosion. During the corrosion and passivity tests, the thickness of the oxide layer with H_2O_2 was determined.

1. Introduction

The tritium in tritiated water decays with the emission of a β^- particle. The energy released in this decay is 5.7 keV per tritium atom. It is high enough to decompose locally the molecules of water along the path of the β^- particle with the formation of hydrogen peroxide. The reactions taking place in the course of this decay are

$$^3H_2O \rightarrow 2^3He + O + 2\beta^- \qquad W = 5.7 \times 2 \text{ keV} \quad (1)$$

$$2H_2O + \beta^- \rightarrow H^\bullet, HO_2^\bullet \rightarrow \text{dissolved } H_2O_2 + 2H \quad (2)$$

To carry out the corrosion and passivity tests, the tritiated water was chemically analysed. The experimental curves were then drawn by cyclic voltammetry, anodic polarization and electrochemical impedance spectroscopy using a carbon steel disc electrode, simulating the conditions in tritiated water, but at different pH and hydrogen peroxide concentrations. The results help in the understanding of the passivity and corrosion in this medium, and in ascertaining the thickness of the oxide layer.

2. Experimental procedure

The voltammetric equipment consisted of a Tacussel bipotentiostat and signal generator (PRT-20 and GSTP3) connected to a Tektronix 2230 digital oscilloscope and a Hewlett–Packard HP 7440 AXY plotter. The impedance diagrams, and anodic polarization curves were drawn by using a ZCP 130 T Tacussel controlled by a 486-25 U Vectra Hewlett–Packard computer using the same plotter. The curves were plotted using 1018 carbon steel with a surface of 0.2 cm^2, whose rotation rate (r.p.m.) was determined in each test. At the rates selected, "noise" in the measurements due to hydrogen or oxygen bubble formation and release, was avoided on the surface of carbon steel. The working electrode potentials were related to a saturated calomel electrode, and a platinum counter electrode was used. To avoid capacitive interferences at the reference electrode, a platinum wire was connected to the reference electrode through a capacitance of 0.1 μF. The impedance measurements were made in the frequency range 10 mHz–100 kHz with a constant a.c. voltage amplitude of 10 mV.

To determine the effect of the pH, it was modified, if necessary, by the addition of H_2SO_4, or NaOH, but not by the addition of buffer solutions. Sodium sulphate was used as a support electrolyte at a concentration of 0.1 mol dm^{-3} to compensate the ohmic drop. The composition of the carbon steel is given in Table 1.

3. Results and discussion

3.1. Voltammograms and polarization curves obtained without H_2O_2

Representative cyclic voltammograms of potential versus current are given which show the behaviour of the carbon steel at pH 13 (Figs 1 and 2), pH 6, 5.5 and 5 (Fig. 2) at a scan rate of 350 mV s^{-1}. The voltammograms were plotted between the potentials of the hydrogen and oxygen evolutions. The stabilized cycles

*Member of the Institute of Corrosion

0022–2461 © 1995 Chapman & Hall

TABLE I Composition (%) of carbon steel

C	P	S	Mn	Fe
0.16	0.006	0.018	0.79	bal.

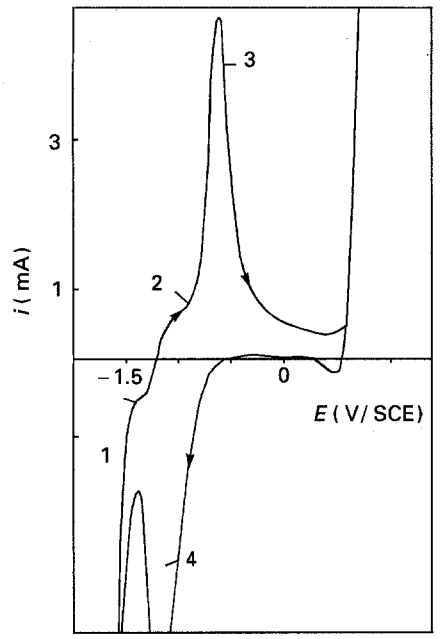

Figure 1 Voltammetry curves of the carbon steel. Na_2SO_4 0.1 mol dm^{-3}, surface 0.2 cm^2, temperature 20 °C, scan rate 350 mV s^{-1}, ω 2000 r.p.m., pH 13.

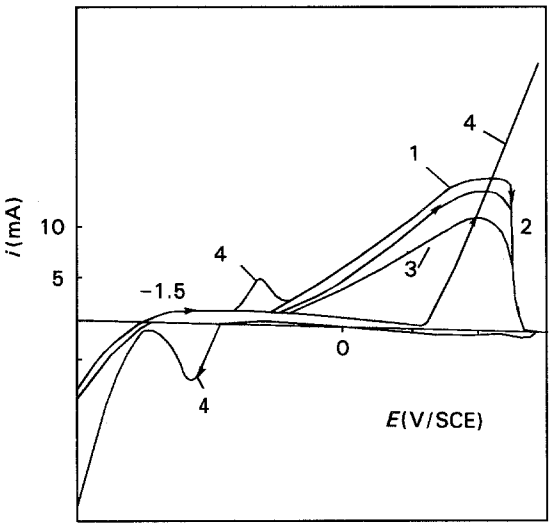

Figure 2 Voltammetry curves of the carbon steel. Na_2SO_4 0.1 mol dm^{-3}, surface 0.2 cm^2, temperature 20 °C, scan rate 350 mV s^{-1}, ω 2000 r.p.m.; (1) pH 5, (2) pH 5.5, (3) pH 6, (4) pH 13.

after multiple, repetitive scannings are seen in the figures. In general, such voltammograms may yield information on electrochemical mechanisms of oxidation and reduction, particularly at high scan rates where adsorbed intermediates can be detected. However, detailed interpretations at high rates are difficult, and complicated by peak potentials which are displaced from their thermodynamic values. Tacconi *et al.* [1] have shown that the potentials, ΔE, obtained from the resistance model, vary linearly with the square root of the potential scan rate in the form

$$\Delta E = [QR_p^2/(dR_p/d\theta)]^{0.5}\Delta v^{0.5} \quad (3)$$

where θ is the degree of coverage, Q is the charge required to cover the carbon steel with a layer of oxide, and R_p is the polarization resistance.

The voltammograms at pH 13 (Fig. 1) show that at the most negative potentials, the currents are cathodic, consistent with hydrogen evolution. On increasing the potential in the forward direction, two minor oxidation peaks (1 and 2) appear as shoulders near − 1.5 and − 1 V/SCE, followed by a major prepassive peak (3) near − 0.65 V/SCE. In the reverse scan, a major reduction peak (4) occurs near − 1.1 V/SCE. Comparison with Schrebler Guzman *et al*'s work [2] suggests that peak (3) involves oxidation from $HFeO_2^-$ to Fe_3O_4, and Fe_3O_4 to γ-Fe_2O_3 leading to the passivity at the higher potentials. Precise interpretation is difficult because the peaks are displaced towards the less-positive potentials due to anodic scan-rate effects. Peak (4) is believed to be a conjugate of peak (3). A straight line drawn between the tops of conjugate peaks (3, 4) suggests this to be close to the "alloy red-ox potential". Comparison with the Pourbaix's diagram of iron [3] shows this to correspond reasonably well with the $Fe_3O_4/HFeO_2^-$ equilibrium, indicating that the major oxide layer related processes in peaks (3, 4) and involves formation and reduction of Fe_3O_4, respectively.

The origin of peak (1) is uncertain. It may be associated with the formation of an adsorbed monolayer of FeOH, $Fe(OH)_2$ or hydrogen [4].

In Fig. 2, still at pH 13 (curve 4), the transpassive current is detected, extending the limit of the anodic potential scan beyond the end of the passive region (potential upon 0.7 V/SCE). According to Beck *et al.* [5], for iron in NaOH solutions at pH 13, the overall reaction concerning the transpassive region is formulated as follows

$$Fe_2O_3 + 10\,OH^- \rightarrow 2\,FeO_4^{2-} + 5\,H_2O + 6\,e^- \quad (4)$$

It is clear that some of the OH^- ions participate in the production of FeO_4^{2-} from Fe_2O_3. Furthermore, this participation is not only in terms of a bulk effect of the oxide layer, but also in terms of an effect on the resistance associated with the oxide and Helmholtz capacitances.

The voltammetric curves in Fig. 2 are also obtained at different pH between 5 and 6, (curves 1–3). The anodic scans show that peaks (1) to (4) in Fig. 1 are missing at these slightly acid pH values. On the other hand, a much higher anodic current is observed in the potential region where carbon steel is passivated at pH 13. This latter figure demonstrates that the steel is easily corroded, as indicated in Pourbaix's diagram for iron [3], leading to Fe^{2+}, Fe^{3+} ions and the oxide layer. These anodic currents increase when the slightly acid pH decreases, and this increase is shifted towards more negative potentials. As a result, cyclic voltammograms using a high scan rate show marked differences at pH 13 and slightly acid pH, and suggest

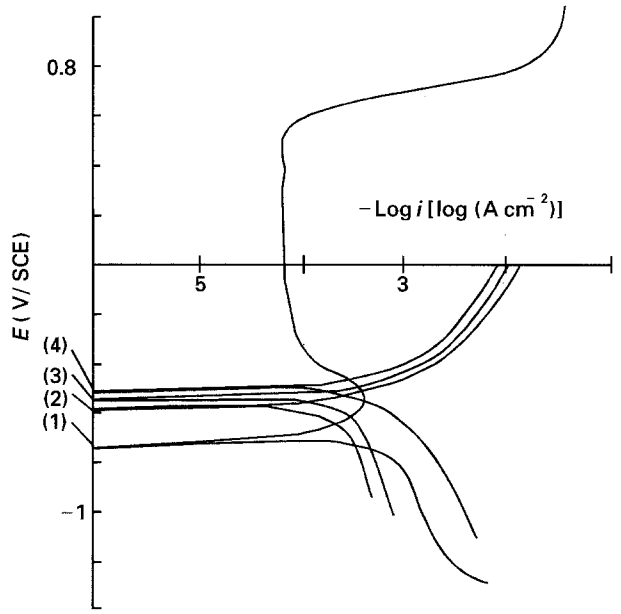

Figure 3 Polarization curves of the carbon steel. Na_2SO_4 0.1 mol dm^{-3}, surface 0.2 cm^2, temperature 20 °C, scan rate 5 mV s^{-1}, ω 2000 r.p.m.; (1) pH 13, (2) pH 6, (3) pH 5.5, (4) pH 5.

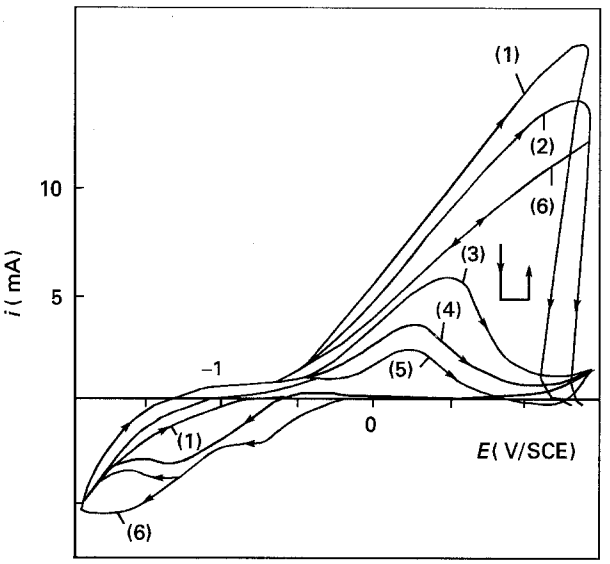

Figure 4 Voltammetry curves of the carbon steel. Na_2SO_4 0.1 mol dm^{-3}, surface 0.2 cm^2, temperature 20 °C, scan rate 350 mV s^{-1}, ω 2000 r.p.m., pH 6. H_2O_2: (1) 10^{-4} mol dm^{-3}, (2) 10^{-3} mol dm^{-3}, (3) 3×10^{-3} mol dm^{-3}, (4) 7×10^{-3} mol dm^{-3}, (5) 10^{-2} mol dm^{-3}, (6) 10^{-2} mol dm^{-3}.

that there is a more protective oxide layer at alkaline pH.

Anodic polarization curves for pH 13, 6, 5.5 and 5, at a low scan rate of 5 mV s^{-1} are presented in Fig. 3. Curve 1 was obtained with NaOH, and shows a prepassive peak at − 0.6 V/SCE. The passive region extends from − 0.4 to 0.65 V/SCE. Curves 2–4 were obtained at slightly acid pH. The prepassive peaks are not seen, on the other hand; the current increases with the potential and as the slightly acid pH decreases. These currents are higher than at pH 13. The values of the corrosion potential increase with decreasing pH, and the experimental slope dE/d pH is about 0.05 mV and close to the slope of a reversible hydrogen electrode. This can be referred to the following cathodic reactions

$$2H^+ + 2e^- \rightarrow 2H \text{ in acid medium} \quad (5)$$

$$2H_2O + 2e^- \rightarrow 2OH^- + 2H \quad \text{in alkaline medium} \quad (6)$$

In anodic polarization curves using a low scan rate, no intermediate shoulders are found; nevertheless, the potential peaks and the passive region are less displaced from their thermodynamic reversible values. This allows us to choose accurate potentials, located, for example, in the passive–transpassive region or near the corrosion potential, in order to draw electrochemical impedance diagrams. These diagrams will be used to find the value of the oxide layer thickness.

3.2. Voltammograms and polarization curves obtained with H_2O_2

Fig. 4 illustrates the voltammetric curves obtained with hydrogen peroxide at pH 6 and a high scan rate. It is evident that the presence of hydrogen peroxide significantly affects the oxidation and reduction processes of carbon steel. After the addition of small amounts of hydrogen peroxide, the height of the oxidation current decreases (curves 1–5) at the potentials at − 0.4 V/SCE. As is shown in curve 6, after several cycles, the curve is again transformed and the current increases. This suggests the thickness of the protective oxide layer is a function of the number of scans, and this progressively changes with scans, a limit being reached [6] in the last scan. In the cathodic scan, the reduction currents increase with the hydrogen peroxide concentration, signifying that the latter is reduced following the cathodic reaction

$$H_2O_2 + 2H^+ + 2e^- \rightarrow 2H_2O \quad (7)$$

Fig. 5 presents several voltammetric curves at a high scan rate illustrating the effect of hydrogen peroxide with sodium hydroxide. On increasing the hydrogen peroxide, peaks 3 and 4 shift towards the more negative currents and peak 3 is not seen at 8×10^{-3} mol dm^{-3} of H_2O_2 (curve 4). On going beyond the passive region, a considerable decrease in anodic current is observed with H_2O_2 giving way to a well-defined transpassive small peak (curve 4). It would appear that the passive oxide layer is more difficult to break down, as can be seen in the passive region where the currents become smaller with hydrogen peroxide.

The explanation of the behaviour of these curves with H_2O_2 is helped by using the diagrams in Fig. 6 and in [7]. At low hydrogen peroxide concentrations, the H_2O_2 reduction currents shift towards negative values. The net current is the oxidation peak in the anodic voltammograms. It is equal to the sum of two currents with opposite signs: that due to the oxidation of the carbon steel and that due to the reduction of the H_2O_2. The corrosion or rest potential should be in the region of potentials of the prepassive peak. For these H_2O_2 concentrations, the corrosion current should be higher (curves 2, 3, Fig. 6) than those obtained in the

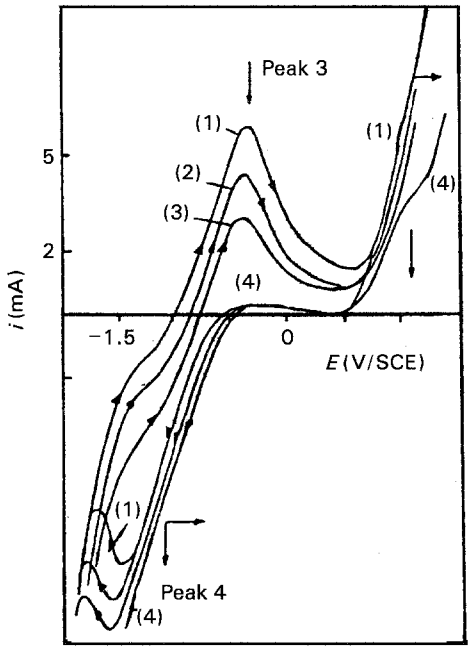

Figure 5 Voltammetry curves of the carbon steel. Na_2SO_4 0.1 mol dm^{-3}, surface 0.2 cm^2, temperature 20 °C, scan rate 350 mV s^{-1}, ω 2000 r.p.m., pH 13. Effect of H_2O_2; (1) 2×10^{-3} mol dm^{-3}, (2) 4×10^{-3} mol dm^{-3}, (3) 6×10^{-3} mol dm^{-3}, (4) 8×10^{-3} mol dm^{-3}.

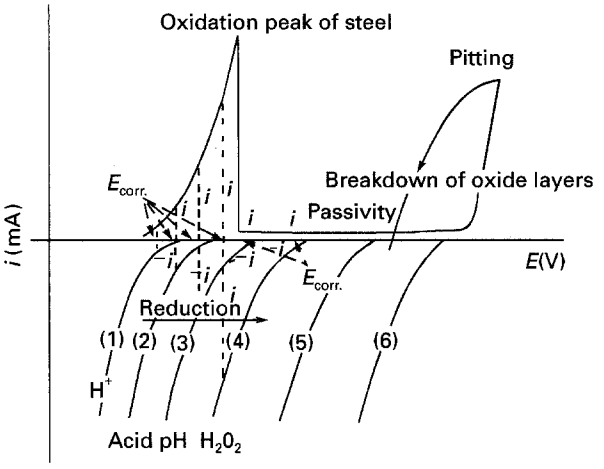

Figure 6 Diagram giving the currents, which have opposite signs, for the oxidation of the steel and the reduction of water and hydrogen peroxide.

absence of H_2O_2 (curve 1, Fig. 6). The behaviour at intermediate hydrogen peroxide concentrations is shown by curve 5 in Fig. 6. In this case, the H_2O_2 reduction currents to be considered are in the passivity potentials and are low. The corrosion potential will be in the passive region and the carbon steel is protected against corrosion. It follows that the passive oxide layer should be more difficult to destroy, as can be seen in the transpassive and passive regions where the currents become smaller. In addition, the characteristics of the oxide layer in slightly acid solution are different from those of the layer formed at pH 13 (curve 6, Fig. 4). In this case, at pH 6, at the same H_2O_2 concentration, the reduction currents to be considered are shifted towards more positive potentials than at pH 13 (H_2O, Pourbaix's diagram [3]).

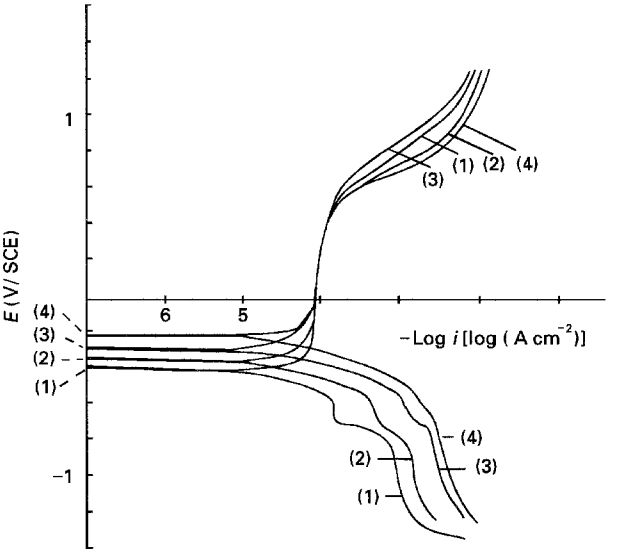

Figure 7 Polarization curves of the carbon steel. Na_2SO_4 0.1 mol dm^{-3}, surface 0.2 cm^2, temperature 20 °C, scan rate 5 mV s^{-1}, ω 2000 r.p.m., pH 13. Effect of H_2O_2: (1) 2×10^{-3} mol dm^{-3}, (2) 4×10^{-3} mol dm^{-3}, (3) 6×10^{-3} mol dm^{-3}, (4) 8×10^{-3} mol dm^{-3}.

In regard to curve 6, Fig. 6 shows that the oxide layer is easily and progressively destroyed with successive cycles. The corrosion potential is in transpassivity. These results could be explained by the pH and the concentration of hydrogen peroxide; the structure or defects of the passive layer should be different with or without H_2O_2.

Anodic polarizations, for pH 13 with hydrogen peroxide, at a low scan rate of 5 mV s^{-1}, are presented in Fig. 7. These curves exhibit different characteristics. Following the increase of the hydrogen peroxide concentration, the passive–transpassive currents (located at 0.6 V/SCE) are higher, then subsequently lower and higher. This is due to the displacement of the corrosion or rest potential towards more positive potentials (located first in the active zone, then in passivity, finally near transpassivity). For example, with concentrations from 2×10^{-3} to 2×10^{-2} mol dm^{-3} H_2O_2, the current increases from 0.2 mA cm^{-2} to 0.8 mA cm^{-2}, the carbon steel is more easily corroded with 2×10^{-2} mol dm^{-3} H_2O_2.

3.3. Impedance spectroscopy without H_2O_2

The impedance diagrams obtained at passive–transpassive potentials for pH 13 are shown in Fig. 8. The Nyquist response is well represented by the capacitive loop. The semicircle with the semicircular arc below the real axis is observed. The interpretation could be that the formation of FeO_4^{2-} (Equation 4) is partly limited by charges within the oxide layer and adsorbates. In the low-frequency region, a loop is seen at higher passive–transpassive potentials, affected by breakdowns of the oxide layer. The loop could be explained by formation of FeO_4^{2-} and adsorbates. As the potentials increase, the transfer resistance decreases considerably from 227 Ω cm^2 at 0.62 V/SCE to 8 Ω cm^2 at 0.7 V/SCE; this is the result of increasing oxidation current.

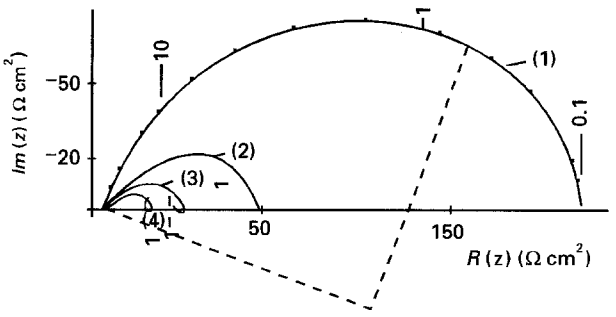

Figure 8 Impedance diagrams of the carbon steel. Na_2SO_4 0.1 mol dm^{-3}, surface 0.2 cm^2, temperature 20 °C, ω 2000 r.p.m., pH 13. Effect of potential: (1) 0.62 V/SCE, (2) 0.65 V/SCE, (3) 0.675 V/SCE, (4) 0.7 V/SCE.

TABLE II Parameters from impedance spectroscopy for transpassive potentials

E(V/SCE)	R_{ct}(Ω cm^2)	C($10^4 \times$ F cm^{-2})
0.62	227	6.4
0.65	50	6.4
0.675	15	6.2
0.7	8	6.6

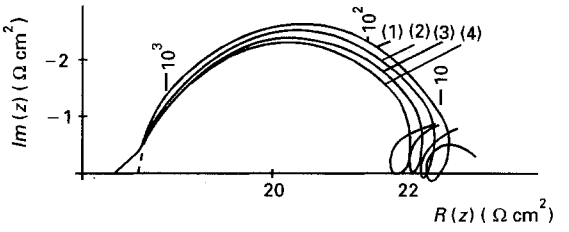

Figure 9 Impedance diagrams of the carbon steel. Na_2SO_4 0.1 mol dm^{-3}, surface 0.2 cm^2, temperature 20 °C, ω 2000 r.p.m., pH 6. Effect of potential: (1) − 0.35 V/SCE, (2) − 0.3 V/SCE, (3) − 0.25 V/SCE, (4) − 0.2 V/SCE.

TABLE III Parameters from impedance spectroscopy for active potentials

	E(V/SCE)			
	− 0.35	− 0.30	− 0.25	− 0.20
R_{ct}(Ω cm^2)	6.3	5.7	5	4
C($10^4 \times$ F cm^{-2})	1.6	1.2	1.1	1

The values of interfacial capacity given in Table II are high. Generally, the Helmholtz capacity is about 20 μF cm^{-2}. The values found can be interpreted as resulting from capacitive effects of carbon steel subjected to a dissolution process seeing that the potentials selected are located at the boundary of the passive–transpassive region. The capacity values do not change with potential. It would appear that this is not a matter of oxide capacitance in which thickness would decrease with the transpassive potentials.

Fig. 9 presents the Nyquist diagrams of carbon steel at pH 6, and Table III gives experimental values of the

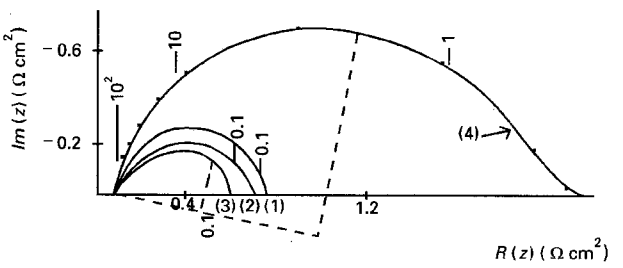

Figure 10 Impedance diagrams of the carbon steel. Na_2SO_4 0.1 mol dm^{-3}, surface 0.2 cm^2, temperature 20 °C, ω 2000 r.p.m., pH 13, E = 0.62 V/SCE. Effect of H_2O_2: (1) 2×10^{-3} mol dm^{-3}, (2) 4×10^{-3} mol dm^{-3}, (3) 6×10^{-3} mol dm^{-3}, (4) 8×10^{-3} mol dm^{-3}.

TABLE IV Transfer resistance and interfacial capacity as a function of H_2O_2 concentration

	H_2O_2($10^3 \times$ mol dm^{-3})			
	2	4	6	8
Z(Ω cm^2)	781	705	629	1857
C($10^3 \times$ F cm^{-2})	2	1.9	0.25	0.05

parameters obtained from the diagrams. The potentials used are located near the corrosion potentials. The interpretation of the relaxation loop at the low frequencies could be that it is due to adsorbates such as FeOH or $Fe(OH)_2$. As the potential increases, the transfer resistance decreases slightly; this is the result of active corrosion. The interfacial capacity values given in the table are also high. The values found can be interpreted as resulting from capacitive effects of carbon steel being subjected to a corrosion process seeing that the potentials selected are located at the boundary of the corrosion potential. The capacity values decrease very slightly with more positive potentials. This could show that there is a corrosion mechanism coupled with slight passivity.

3.4. Impedance spectroscopy with H_2O_2

The Nyquist diagrams obtained at 0.62 V/SCE, pH 13, with hydrogen peroxide at concentrations from 2×10^{-3} to 8×10^{-3} mol dm^{-3} are shown in Fig. 10. The potential chosen would appear to be near the rest potential located in the passive–transpassive region. The diagrams show a decreasing impedance. On the other hand, for 8×10^{-3} mol dm^{-3}, the impedance value is much higher. These two types of behaviour are confirmed by the voltammograms and anodic polarization curves in the passive–transpassive region (Figs 5 and 7). As shown in Fig. 6, at 2×10^{-3} to 6×10^{-3} mol dm^{-3} H_2O_2, the corrosion current should be higher. At 8×10^{-3} mol dm^{-3} H_2O_2, the corrosion potential shifts and will be in the passive region; therefore, the carbon steel is protected against corrosion. It follows that the passive oxide layer should be more difficult to destroy, as can be seen in the impedance values with the same concentration of hydrogen peroxide. Experimental values are given with H_2O_2 concentrations in Table IV.

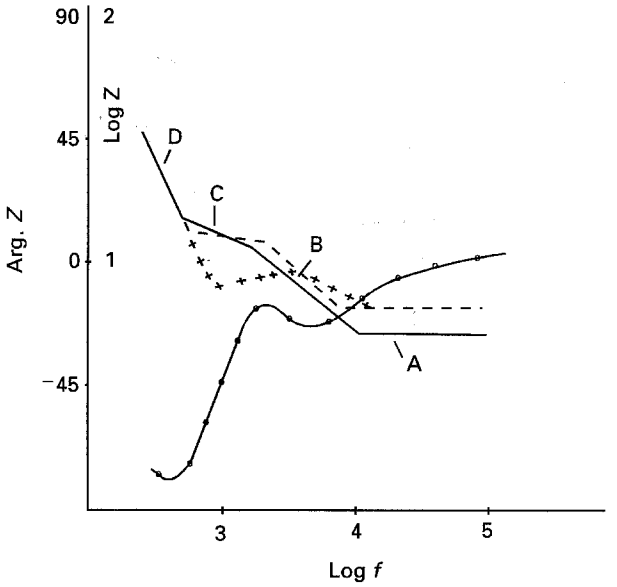

Figure 11 Electrochemical impedance spectroscopy, Bode diagrams. Na_2SO_4 1 mol dm^{-3}, surface 1 cm^2, pH 11. Effect of H_2O_2 impedance module: (——) without H_2O_2, (– – –) 2×10^{-3} to 8×10^{-3} mol dm^{-3}, (+) 5×10^{-2} mol dm^{-3} H_2O_2. (–O–) phase module.

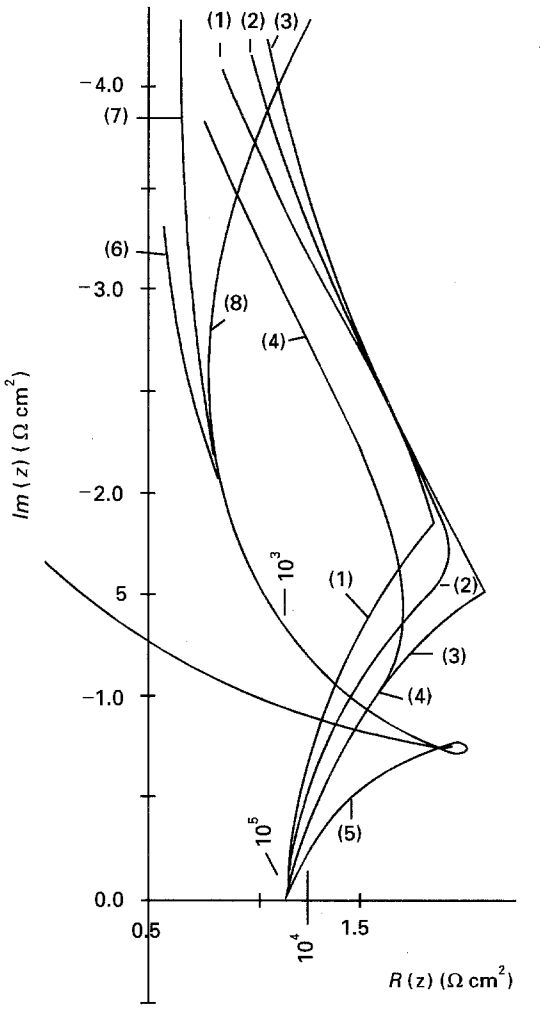

Figure 12 Electrochemical impedance spectroscopy, Nyquist diagrams. Na_2SO_4 1 mol dm^{-3}, surface 1 cm^2, pH 11, 0.3 V/SCE. Effect of H_2O_2: (1) without H_2O_2, (2) 10^{-3} mol dm^{-3}, (3) 2×10^{-3} to 4×10^{-3} mol dm^{-3}, (4) 8×10^{-3} mol dm^{-3}, (5) 10^{-2} mol dm^{-3}, (6) 2×10^{-2} mol dm^{-3}, (7) 3×10^{-2} mol dm^{-3}, (8) 4×10^{-2} mol dm^{-3} H_2O_2.

These values show that the interfacial capacitance decreases significantly with the H_2O_2 concentration. For 2×10^{-3} to 6×10^{-3} mol dm^{-3} H_2O_2, there would appear to be a corrosion mechanism coupled with passivity as can be seen in Fig. 6, curves 3 or 4. For 8×10^{-3} mol dm^{-3} H_2O_2, the value of the capacity (50 μF cm^{-2}) would certainly be the oxide and Helmholtz capacities, indicating that the passivity would be achieved, and this is in agreement with curve 5 in Fig. 6.

Fig. 11 shows the Bode plot of the passive oxide layer at 0.3 V/SCE with different H_2O_2 concentrations between zero and 3×10^{-2} mol dm^{-3}. The diagrams were obtained using fairly high electrolytic conductivity and a small gap between the reference and working electrodes. From the interpretation of Gebhardt [8], the impedance module can be analysed as follows. Segment A is characterized by the pure electrolyte resistance at the highest frequencies. Segment B appears when the frequency decreases, and the electrical response is the impedance of the total oxide marked by non-dissipative characteristics. The slope of segment B may be -1, and in our case the very small slope may be attributed to the superposition of the real impedance. At a lower frequency, segment C appears and the slope is again negative without hydrogen peroxide or up to 8×10^{-3} mol dm^{-3} H_2O_2; the real impedance may again play a role here. At concentrations up to 8×10^{-3} mol dm^{-3}, the slope is zero; near the theoretical value, the effect of real impedance is lower. In segment C, a highly dissipative component of the oxide can be assumed. Segment D is characterized by a long straight impedance with a slope of about -1, and would appear to correspond here to Warburg diffusion in a Nyquist plot; thus a more compact oxide can be assumed. For segment B, it is difficult to calculate the thickness of non-dissipative insulating oxide as shown elsewhere [8, 9]; therefore, we have drawn the Nyquist diagrams (Fig. 12). The capacitive branches tend towards infinity from the high frequencies down to 10^{-2}. The electron diffusion within the oxide may control the kinetics; the charge transfer and ionic diffusion within the oxide layer are less limiting. The Warburg line shifts towards higher real impedance with lower values of hydrogen peroxide meaning less passivity, furthermore the electrolyte becomes yellow; the corrosion potential may be near the intermediate peak. At medium values of hydrogen peroxide, the Warburg line shifts towards negative real impedance (e.g. 10^{-2} mol dm^{-3}) and a loop is seen at the intersection of the semicircle and Warburg line; these suggest a relaxation. At these concentrations of H_2O_2, carbon steel is passivated. At higher values of H_2O_2, the Warburg line tends toward higher values of the real impedance, meaning more corrosion, the corrosion potential may be in the transpassive region (and the yellow colour of electrolyte deepens). The semicircular arcs overlap the Warburg line, and the diameter decreases with the concentration of hydrogen peroxide. With respect to the semicircle, we have estimated the impedance module. The capacitance is calculated

using $C = (2\pi fZ)^{-1}$ and helps to explain the highly non-dissipative insulating character of the oxide layer. The thickness of this, for a plane area, can be obtained from

$$e = \varepsilon\varepsilon_0 A/C \quad (8)$$

where e denotes the thickness of the insulating oxide, A the area, ε_0 and ε the absolute and relative dielectric constants, respectively. The value is about 0.3 nm; the apparently small thickness does not really change with H_2O_2. We assume that the ionic diffusion and holes may also play a role, as is seen with the shift of the Warburg line.

4. Conclusions

In the transpassive–passive region, the oxide layers formed on carbon steel at slightly acid pH, with or without hydrogen peroxide, would not appear to be semiconducting. The passivity occurs mainly at pH 13, while at slightly acid pH, an oxidation current is observed at higher potentials. The observed dependence of the current associated with hydrogen peroxide reduction on the oxide layer would seem to suggest a better passivity at a medium concentration of H_2O_2. The corrosion potential may be located in the passive region. The thickness is calculated at the passive potential; this should protect the carbon steel.

Acknowledgement

The author thanks Professor Rameau, CREMGP, ENSEEG, University of Grenoble, France, for his keen interest in this work.

References

1. M. R. DE TACCONI, A. J. CALANDRA, A. J. ARVIA, *Electrochim. Acta* **18** (1973) 571.
2. R. S. SCHREBLER GUZMAN, J. R. VILCHE and A. J. ARVIA, *J. Appl. Electrochem.* **11** (1981) 551.
3. M. POURBAIX, "Atlas *d'Equilibres Electrochimiques*", ed. Gauthiers Villas (Pergamon Press, Paris 1963).
4. G. BELLANGER, Doctoral thesis, Dijon, France (1989).
5. F. BECK, R. KAUSS and M. OBERST, *Electrochim. Acta* **30** (1985) 173.
6. C. SARASOLA, T. FERMANDEZ and Y. JIMENEZ, *Electrochim. Acta* **33** (1988) 1295.
7. G. BELLANGER, *J. Nucl. Mater.*, **210** (1994) 63.
8. GEBHARDT. *Electrochim. Acta* **38** (1993) 633.
9. G. BELLANGER, "Fusion Technology", *J. Am. Nucl. Soc.*, January 1995.

Received 7 January
and accepted 5 September 1994